Environmental Technology & Innovation 21 (2021) 101292

Contents lists available at ScienceDirect

Environmental Technology & Innovation

journal homepage: www.elsevier.com/locate/eti

Removal of pyridine using ultrasound assisted and conventional batch adsorption based on tea waste residue as biosorbent

Gaurav B. Daware, Parag R. Gogate *

Department of Chemical Engineering, Institute of Chemical Technology, Mumbai 400019, India

ARTICLE INFO

Article history:
Received 27 May 2020
Received in revised form 30 November 2020
Accepted 2 December 2020
Available online 5 December 2020

Keywords:
Pyridine removal
Ultrasound
Tea waste residue (TWR)
Batch adsorption
Kinetic and thermodynamic parameters
Adsorption isotherms

ABSTRACT

The current study deals with comparison of ultrasound assisted adsorption and conventional batch adsorption using biosorbent based on tea waste residue (TWR) with an objective to develop novel treatment approach for effective removal of pyridine. The characterization of TWR was performed using FTIR and SEM to get clear insight into the associated functional groups and the morphology. In addition, point of zero charge was also established and oxygen functional groups were detected using Boehm titration method. Ultrasound assisted adsorption was studied in ultrasonic bath (25 kHz frequency) under varying conditions of pH (2–10), TWR dose (0.5–4 g/L) treatment time (0 to 120 min for ultrasound assisted and 0 to 200 min for conventional approach), temperature (283 K–313 K), power (15 W–150 W) and initial concentration (10 mg/L–150 mg/L). Maximum removal and pyridine uptake obtained for ultrasound assisted adsorption was 98.2% and 37.38 mg/g respectively at optimized conditions of pH of 6, TWR loading of 2.5 g/L, temperature of 303 K, treatment time of 90 min and power of 120 W. Conventional batch adsorption studies performed at fixed 150 rpm as shaking speed revealed that maximum removal and maximum pyridine uptake was obtained as 92.25% and 33.72 mg/g respectively under similar optimum conditions but in treatment time of 160 min required to reach equilibrium. Pseudo second order kinetic model was the best fit for both adsorption approaches. Langmuir adsorption isotherm model for conventional batch adsorption and both Langmuir and Temkin isotherm for ultrasound assisted adsorption were also found suitable. Thermodynamic parameters as ΔG, ΔH and ΔS were evaluated for both adsorption approaches and it was established that the ΔG and ΔS values for ultrasound assisted adsorption for all temperatures and isotherms are higher compared to conventional batch adsorption. Overall, ultrasound was demonstrated as effective means to improve adsorption leading to enhanced extent of adsorption and lower treatment time.

1. Introduction

In recent years, the effluents from various industrial sectors like metallurgical, chemical, mining, fertilizer, nuclear, agriculture, shipping, textile are big concerns for the human health and environment (Nekouei et al., 2015; Burakova et al., 2018; Gupta and Gogate, 2015; Saravanan et al., 2013a,b) and there is an increasing awareness for tackling the pollution.

* Corresponding author.
E-mail address: pr.gogate@ictmumbai.edu.in (P.R. Gogate).

https://doi.org/10.1016/j.eti.2020.101292
2352-1864/

The increase in population which affects badly the quality of water due to significant effluent generation as well as the ever increasing need for fresh and safe water is augmenting the problem that need to be managed properly to maintain proper ecosystem of environment and civilization (Saleh and Gupt, 2014; Saravanan et al., 2013a,b; Gupta et al., 2013; Ahmaruzzaman and Gupta, 2011). The treatment of wastewater is considered as hot research area due to scarcity of fresh and safe water (Saleh and Gupt, 2012; Aruna et al., 2020). One of the major contaminants leading to environmental problems is pyridine or its derivatives that can be present in effluents from many sectors.

Pyridine is naturally occurring aromatic organic compound (chemical formula as C_5H_5N and molar mass = 79.1 g/mole) having wide industrial applications as feed stock, intermediate and solvents in pesticides, oil, fertilizer, pharmaceutical and rubber industries as well as in laboratories (Kumar et al., 1995). It is soluble in water and has colourless appearance. The density of pyridine is 0.098 g/cm^3 and boiling point is 388.2 K. United States Environmental Protection Agency [USEPA] has ranked pyridine higher among the tremendously risky compounds to the environment including the living organisms (Daware and Gogate, 2020a,b). Industrial wastewater typically can have concentrations of pyridine in wastewater as 20 to 300 mg/L though emergency spillage can increase its concentration to considerably greater level (Daware et al., 2014). The maximum concentration of pyridine in treated water that is allowed as per the norms is only 5 mg/L (Daware and Gogate, 2020a,b). Wide industrial applications can lead to occurrence of pyridine or its derivatives in environment for longer durations and its toxic nature necessitates developing treatment methods for removal of pyridine from wastewater. Different methods have been proposed as ultrasonic degradation (Elsayed, 2015), ozonation (Stern et al., 1997), ion exchange (Akita and Takeuchi, 1993), microbial degradation in fuel cell (Zhang et al., 2009), biodegradation (Bai et al., 2009), microwave irradiation (Zalat and Elsayed, 2013) and adsorption (Mohan et al., 2004; Gupta et al., 2015). Different applied treatment approaches have limitations like biodegradation is time consuming and difficult technique requiring good understanding of the operation and appropriate maintenance of microorganisms. Microbial fuel cell process is costly and functioning limitations as restricted operating temperature giving slower rates of degradation. Advanced oxidation process (AOP) has limitations of generation of toxic intermediates, the higher treatment costs for the process and incomplete mineralization of toxic compounds (Shahnaz et al., 2020). Use of only ultrasound for complete degradation again can give much higher treatment costs. Adsorption offers advantages over other methods like more efficient, flexible, and economical approach as well as ease of operation (Gupta et al., 2013; Janani et al., 2019; Saravanan et al., 2012). The application of ultrasound in adsorption at mild intensity can further intensify the operation giving higher removal of the pollutant and reduction in the time of operation. Though the adsorption is handy process still it is highly depends upon the adsorption capacity as well as recycling ability of the adsorbent as well the cost of adsorbent (Jampa et al., 2020). Considering this analysis, the current work has focused on the development of low cost biosorbent and its application for the removal of pyridine using conventional batch adsorption with intensification studies based on the use of ultrasound.

Biosorbents are promising, easily available and low cost adsorbents being applied for efficient removal of hazardous chemicals. Various biosorbents used for efficient elimination of pyridine or its derivatives from wastewater are bagasse fly ash (Lataye et al., 2006), rice husk ash (Lataye et al., 2009) and activated carbon developed from coconut shell (Mohan et al., 2005). Tea waste is another bio-waste abundantly available based on the large consumption of tea powder globally in households, restaurants and industries. Tea waste is available at almost zero material cost and excellent adsorption capacity can be obtained for the removal of hazardous chemicals. Application of tea waste as biosorbent is indeed reported for the removal of dyes (Pirbazari et al., 2014), heavy metals (Malkoc and Nuhoglu, 2006), and phenol (Girisha et al., 2017) from wastewater though no application could be seen for pyridine. Based on this analysis, tea waste residue (TWR) has been selected for adsorptive removal of pyridine in the current work. Literature analysis revealed TWR as adsorbent has not been used for removal of pyridine from wastewater and also the adsorption work reported earlier for removal of pyridine from wastewater is only based on the conventional batch method. Ultrasound based adsorption methodology has not been used for removal of pyridine using any adsorbent in the literature. Use of ultrasound for intensifying the batch adsorption and its comparison in terms of percentage removal, feasibility, spontaneity with conventional batch adsorption has been studied in present work which clearly establishes the novelty of present work.

Ultrasound can enhance the adsorptive removal of pollutant due to the cavitating effects. Ultrasound induced cavitation improves the mass transfer in solid liquid system, enhances available active surface area and also helps in cleaning of solid particles. One of the physical effects of cavitation is generation of turbulence near the solid particles which results in higher rates of mass transfer and also cleaning action. There have been some studies related to the use of ultrasound assisted adsorption for improved efficiency. Milenkovic et al. (2009) reported that ultrasound assisted adsorption of copper ions using ultrasonic bath resulted in enhanced removal of copper in the presence of ultrasound (300 mmole/g) whereas in absence of ultrasound less removal (200 mmole/g) on hazelnut shell activated carbon observed. Landi et al. (2010) also reported that adsorptive removal of phenol on granular activated carbon using ultrasound was 40% and only 25% in the absence of ultrasound, clearly confirming that the treatment was more efficient in the presence of ultrasound. Gupta and Gogate (2015) also reported that the extent of removal of copper using watermelon shell as adsorbent was higher (90% extent of removal in 20 min) in the presence of ultrasound compared to conventional batch adsorption (86% removal in 60 min).

Analysis of the literature clearly established that the current work is first approach of utilization of tea waste residue (TWR) for pyridine removal both in the ultrasound assisted adsorption and also conventional adsorption clearly establishing the novelty. The effect of different parameters like power, pH, adsorbent loading, time, temperature and initial concentration on the removal of pyridine has also been studied. In addition, FTIR analysis of TWR before and after

adsorption of pyridine has been performed to establish the governing mechanism for adsorption. The kinetics, isotherm and thermodynamic studies were also performed to obtain the important design information. The work also focused on the comparison of ultrasound assisted and conventional batch adsorption approaches so as to quantify the process intensification benefits.

2. Materials and methodology

2.1. Materials

Pyridine was purchased from Sigma-Aldrich [Now Merck India], Mumbai. Synthetic wastewater was prepared by adding pyridine at required concentration in distilled water for the study. Tea waste residue (TWR) was obtained from local tea shop and sieved over the size range of 200 to 250 μm. TWR was washed with boiling water repeatedly to remove caffeine and tannin, present in residue. The obtained TWR was dried in oven at 353 K for 24 h. The dried TWR was then treated with 0.1N NaOH solution for 10 h to remove colour imparting impurities. Subsequently the sample was washed with distilled water continuously till neutralization, dried in oven at temperature of 343 K for 36 h and then stored for the use in the experimentation.

2.2. Methodology

The experiments for ultrasound assisted adsorption were performed in 8 L capacity ultrasonic bath operating at fixed frequency of 25 kHz. The ultrasonic bath is typical cleaning tank type vessel with dimensions of 300×180×150 mm. The operational parameters (temperature, time, power) can be set using a control panel. The tank is also provided with a drainage facility at the bottom.

Experiments were typically conducted using pyridine containing wastewater of specific concentration and 100 mL volume taken in 200 mL flask. Effect of different operating conditions as ultrasonic power (15 W–150 W), TWR loading (0.5–4 g/L), initial concentration (10 mg/L–150 mg/L), pH (2–10), temperature (283 K–313 K) and time (0 to 120 min) on the pyridine removal have been investigated. The pH of pyridine solution was adjusted using 0.1N NaOH or 0.1N H_2SO_4 solution as required. The pyridine solution was also continuously stirred using mechanical stirrer at 150 rpm.

Conventional batch adsorption experiments were performed using thermostatic shaker incubator (Biotechnics, India) with working solution of 100 mL taken in 200 mL conical flask. A constant agitation speed of 150 rpm was used and influence of various operating conditions like temperature (283 K–313 K), time (0 to 200 min) and initial pyridine concentration (10 mg/L–150 mg/L) at optimized pH and TWR loading (established based on ultrasound assisted adsorption experiments) has been investigated. During the ultrasound assisted and conventional batch adsorption studies, the samples of pyridine solution were collected at preselected time intervals, centrifuged and analysed to identify unabsorbed pyridine using UV spectrophotometer (Shimadzu Model) operated at 254 nm wavelength. Pyridine uptake on TWR was evaluated using the following equation (Gupta et al., 2011)

$$q_e = \frac{c_i - c_e}{w} \tag{1}$$

Where, c_i and c_e are the initial and equilibrium concentration of pyridine (mg/L) and w is TWR loading (g/L) applied for experiments.

3. Results and discussion

3.1. Characterization

The characteristic functional groups on the adsorbent are identified based on the FTIR spectra. Fig. 1(a) and Fig. 1(b) represents the FTIR spectra of TWR in the native form and after use for pyridine adsorption. The observed peak at 3350 cm^{-1} corresponding to N–H group shifted to 3331 cm^{-1} after adsorption showing N–H interaction during adsorption on TWR (Alam and Kamaluddin, 2000). The peak before adsorption at 1438.30 cm^{-1} shifted to 1442.75 cm^{-1} establishing clear role of single C–N bond in the adsorption (Lataye et al., 2008a,b). The peak before adsorption identified at 1625.99 cm^{-1} also shifted to 1639.9 cm^{-1} due to NH deformation and R-NH bending vibration (Lataye et al., 2008a,b). It can be thus said that the FTIR spectra before and after use in the adsorption allowed establishing the role of different functional groups and also confirming the adsorption of the pyridine molecule on TWR.

The morphology of TWR was studied before and after adsorption using SEM analysis (Zeiss Model 108). SEM image obtained before adsorption (Fig. 2(a)) showed the fibrous, porous and uneven structure of TWR while Fig. 2(b) SEM image obtained after adsorption revealed the change in morphology due to penetration of pyridine molecules into the pore and also adsorption over the surface.

Point of zero charge of TWR was calculated by changing pH from 1 to 10. When the pH value is greater than the point of zero charge (pH_{PZC}), the surface of adsorbent is having negative charge while at pH values lesser than pH_{PZC}, the surface of adsorbent is having positive charge. The point of zero charge was estimated by using pH drift method (Bhandari and

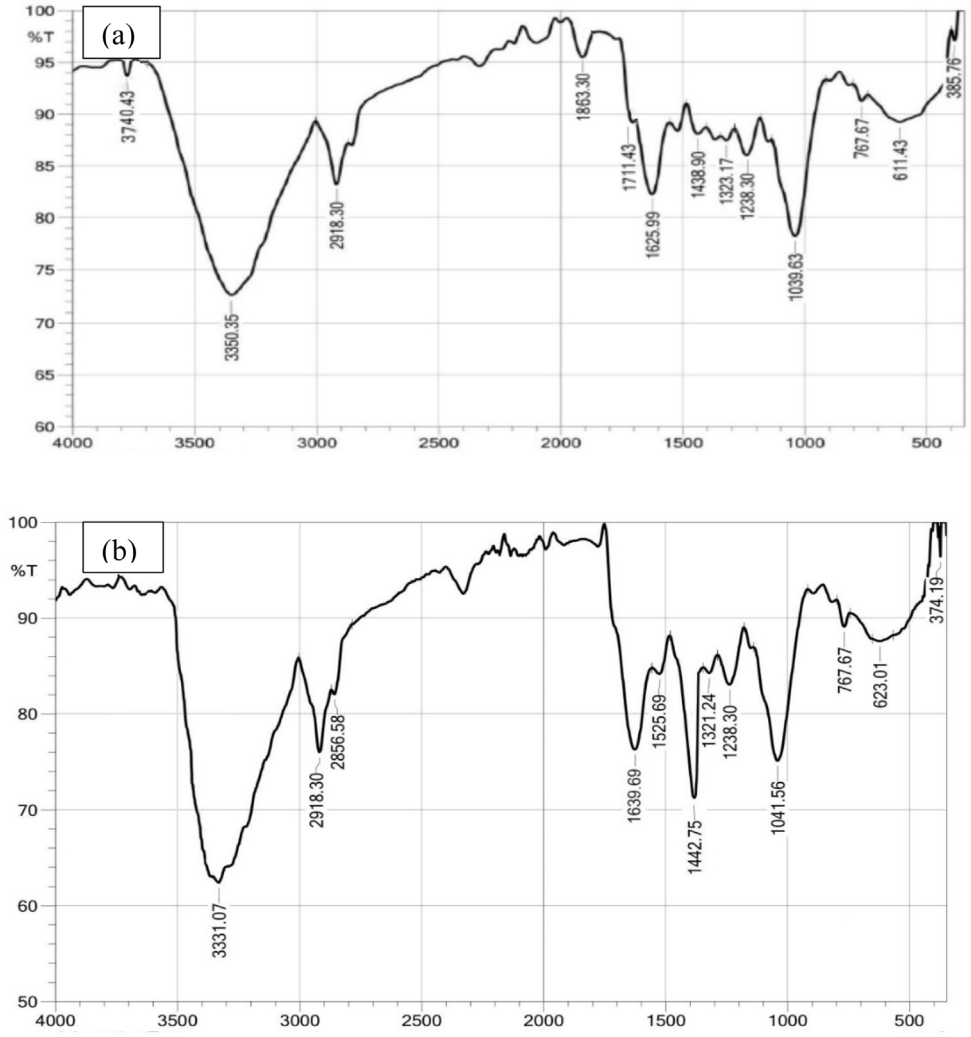

Fig. 1. FTIR spectra of TWR (a) before pyridine adsorption and (b) after pyridine adsorption.

Gogate, 2018). The NaCl solution was prepared of strength 0.01N and 0.1 g of TWR was added in 50 mL of NaCl solution. The initial pH of the NaCl solution was recorded as pH initial. The different flasks of solutions with different pH (1 to 10) were kept in orbital shaker at speed 150 rpm for 24 h. The pH of 0.01 NaCl solution in all the flask after 24 h treatment was measured as the final pH (pH final). Graph was plotted of pH final of NaCl solution containing TWR against the pH initial of NaCl solution containing TWR as shown in Fig. 3. It can be seen from the figure that at 6.6 the initial value and final value are same which is considered as point of zero charge of TWR. The TWR surface will be positively charged till 6.6 and beyond it, the surface will be negatively charged.

The quantum of oxygen containing functional group was analysed using Boehm titration method (Boehm, 2002; Fidel et al., 2013). Three reaction bases as $NaHCO_3$, Na_2CO_3 and NaOH solution of 0.01 N concentration were prepared. 0.1 g of TWR was added in three conical flasks and 50 mL of the prepared 0.01 N base ($NaHCO_3$, Na_2CO_3 and NaOH) was also added to each conical flask containing TWR. The samples were properly sealed and transferred to orbital shaker incubator for shaking for 72 h. After the treatment, the TWR was separated from the solution using Whatman filter paper. The base samples of $NaHCO_3$ and NaOH of 10 mL volume and Na_2CO_3 of 20 mL volume each were then transferred to different flasks. The samples heated to 106 °C to remove CO_2. Afterwards the samples were back titrated against 0.01N NaOH solution. The base samples of 0.01N strength ($NaHCO_3$, Na_2CO_3 and NaOH) without TWR served as the blank samples.

The functional group concentration were determined using following equations (Fidel et al., 2013)

$$n_{(Cg)}\left[\frac{\text{mmole}}{\text{gm}}\right] = \frac{(V_{sample} - V_{blank})}{m} \times CT \times DF \tag{2}$$

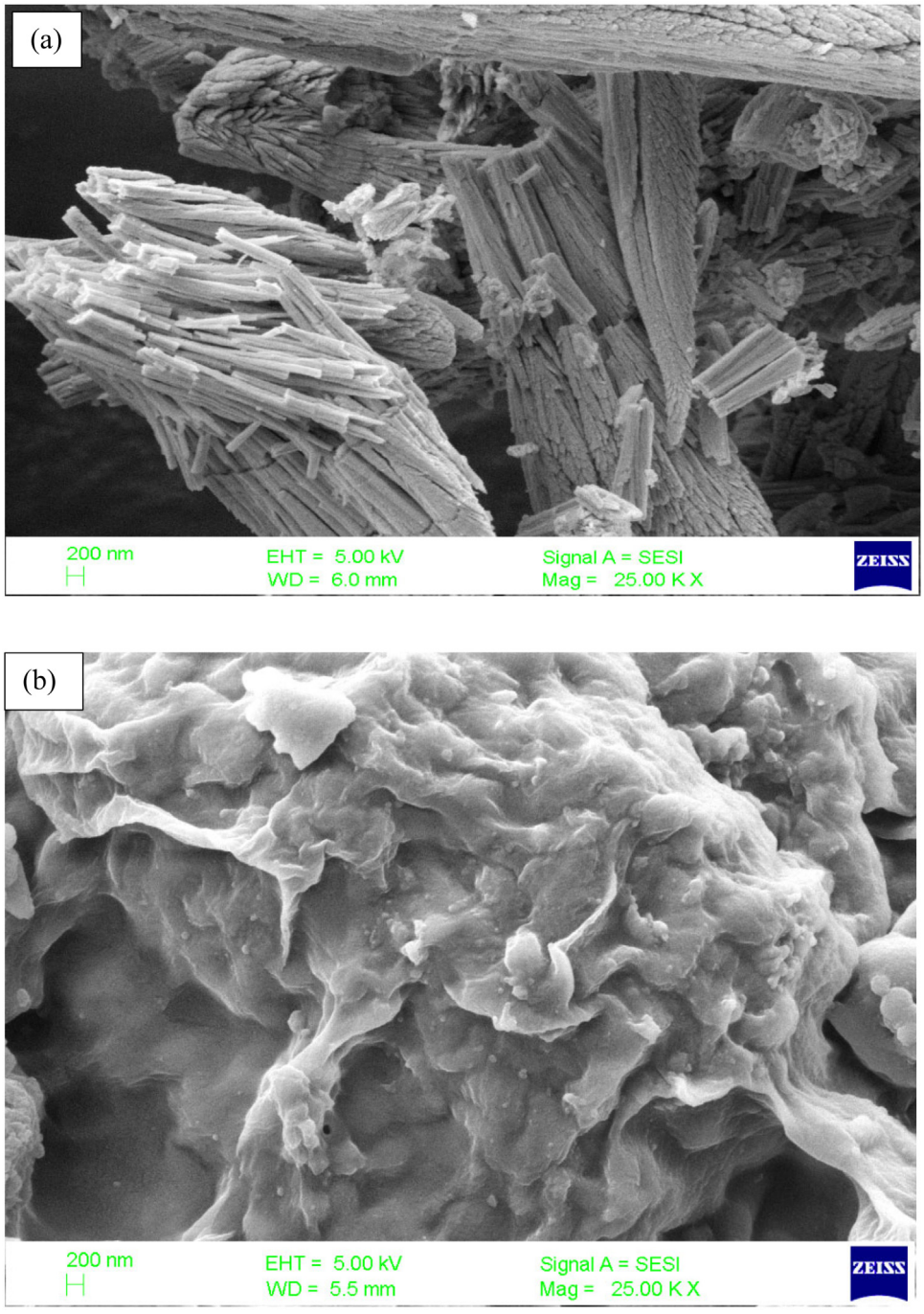

Fig. 2. SEM images (a) before pyridine adsorption and (b) after pyridine adsorption.

$$n_{(Lg)}\left[\frac{\text{mmole}}{\text{gm}}\right] = \left(\frac{(V_{sample} - V_{blank})}{m} \times CT \times DF\right) - n_{(Cg)} \tag{3}$$

$$n_{(Ph)}\left[\frac{\text{mmole}}{\text{gm}}\right] = \left(\frac{(V_{sample} - V_{blank})}{m} \times CT \times DF\right) - (n_{(Cg)} + n_{(lg)}) \tag{4}$$

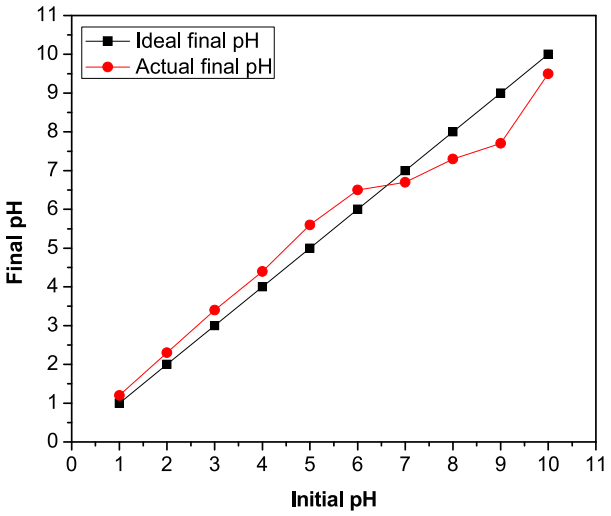

Fig. 3. Point of zero charge of TWR.

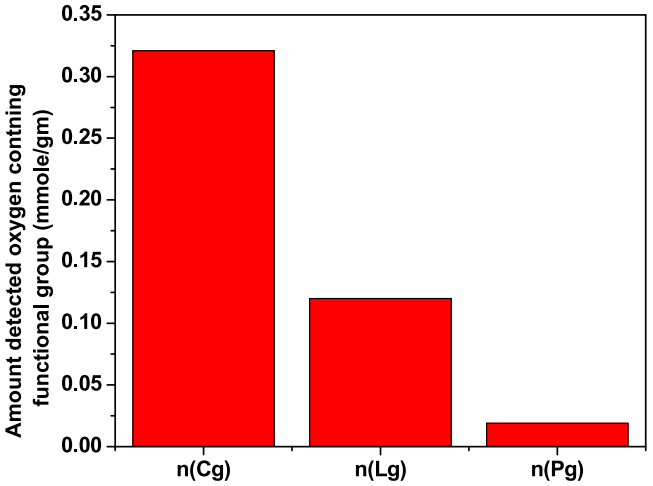

Fig. 4. Oxygen functional groups using Boehm titration method.

$n_{(Cg)}, n_{(Lg)}$ and $n_{(Ph)}$ refers to the carboxylic group, lactone group and phenolic group, respectively. *CT* is concentration of titrant is expressed in mole/L, DF referees to Dilution factor and m is the g of TWR. The obtained quantities of $n_{(cg)}$, $n_{(lg)}$ and $n_{(Ph)}$ were 0.3210 mmole/g, 0.1201 mmole/g and 0.0119 mmole/g respectively and hence the total quantity of oxygen containing functional group for TWR is 0.4530 mmole/g. The reported results are represented in Fig. 4. Kalijadis et al. (2011) reported similar kind of results for activated carbon using Boehm method.

3.2. Ultrasound assisted batch adsorption study

3.2.1. Influence of ultrasonic Power on pyridine removal

The dependency of extent of removal of pyridine on ultrasonic power dissipation was studied at different power (15–150 W) with the obtained results given in Fig. 5. It can be seen from the data that the extent of adsorption enhances from 39.5% to 94% with an increase in operating power from 15 W to 120 W under conditions of pH 6, time of 90 min, temperature of 303 K, initial pyridine concentration as 50 mg/L and TWR loading of 2.5 g/L. An increase in power enhances the mixing and turbulence resulting in enhanced mass transfer and hence higher extent of pyridine removal (Gogate et al., 2011). It was also seen in the work that the observed pyridine removal as 94% at power of 120 W only marginally increased to 95.7% with a further increase in power to 135 W and subsequently to 96.4% for ultrasonic power dissipation of 150 W. The trends clearly imply that very less increase in pyridine removal is observed over the power range of 120 W–150 W establishing 120 W as the optimum. It can be said that beyond the optimum, decoupling losses reduces the energy

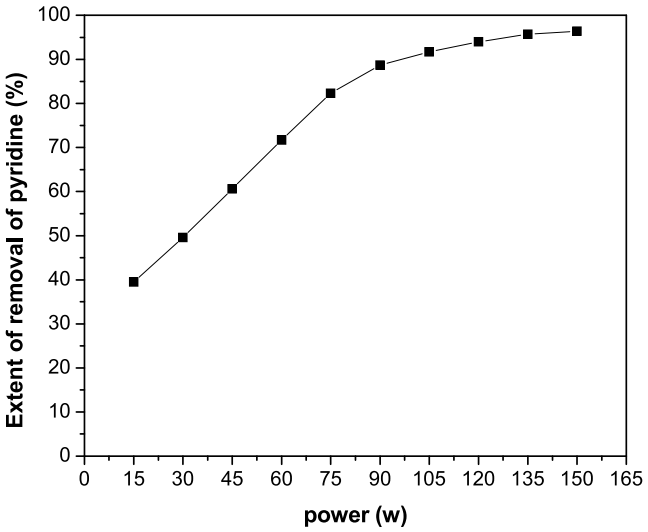

Fig. 5. Effect of power on the extent of removal of pyridine using Ultrasound assisted adsorption (T = 303 K, t = 90 min, c_i = 50 mg/L, w = 2.5 g/L).

transfer and hence the intensity of cavitation effects, yielding only a marginal increase (only by 2.4%) in the extent of removal of pyridine. Considering the observed trends, further adsorption studies were performed at 120 W as the selected power dissipation. Similar trends can be seen in literature though with different quantitative value of optimum power dissipation. Gupta and Gogate (2015) reported similar trends for adsorption of metal on watermelon based biosorbent with the removal increasing from 35% to 87% for an increase in power from 20 W to 90 W but a further increase in power to 100 W resulted in very less increase in the metal removal using biosorbent.

3.2.2. Influence of pH on pyridine removal

The adsorption of any pollutant strongly depends on the operating pH and hence the influence of pH on pyridine removal was also studied for ultrasound assisted adsorption. Pyridine is weak base as nitrogen atom is having negative charge and has a pKa value of 5.23 (Gero and Markham, 1951). The extent of removal of pyridine was studied by changing the value of pH from 2–10 by keeping other operative parameters at constant values. The observed results in terms of extent of removal and the amount of pyridine adsorbed per unit g of TWR at equilibrium are shown in Fig. 6(a) and Fig. 6(b) respectively. The maximum extent of removal of pyridine on TWR was 94.1% and amount of pyridine adsorbed on TWR was 18.8 mg/g at pH of 6. In terms of the observed trends, extent of removal of pyridine increased from 48.2 to 94.1% and the amount of pyridine adsorbed on TWR from 9.64 to 18.8 mg/g with a change in pH of pyridine solution from 2 to 6. At highly acidic conditions (lower pH values) the pyridine is converted into PyH^+ form due to protonation based on existing lone pair on nitrogen as shown by following reaction:

$$Py + H^+ \longrightarrow PyH^+$$

The protonated form offers less interaction with the adsorbent surface giving lower removal compared to the neutral form at pH of 6. It was also observed that subsequently increasing the pH from 7 to 10 lead to lower extent of removal as 86.1% with amount of pyridine adsorbed as 17.41 mg/g. The observed trends can be explained on the basis of the point of charge of TWR which is 6.6. As pyridine molecule contains more electronegative atoms (N) than sp^2 hybridized atom (C) that are mostly adsorbed on positive charge surface, higher removal is obtained at pH of 6. Beyond pH of 6.6, inefficient interaction based on the charge leads to lower extent of removal. Xia et al. (2018) reported similar results for pH influence on adsorption of pyridine on lignosulfonate intercalated hydroxide. It was shown that pyridine adsorption increases from 71 mg/g to 140 mg/g with an increase in pH from 3 to 6 but subsequent increase in pH to 12 leads to a lower pyridine adsorption as 98 mg/g. Lataye et al. (2006) also reported that the extent of removal of pyridine using bagasse Fly ash increased from 78% to 93.7% on increasing pH from 2 to 6 but at pH above 6, lower removal of pyridine (86.7%) was seen. Though the trends are similar, there exist quantitative differences in the removal extents thereby confirming the importance of the work. Considered the obtained results in the current work, further experiments were performed by keeping pyridine solution pH constant at 6.

3.2.3. Influence of TWR adsorbent loading

Proper choice of adsorbent loading is vital as the available surface area and sites influences the adsorption effectiveness. The effect of loading of TWR over the range of 0.5–4 g/L on the removal of pyridine was studied using 50 mg/L pyridine

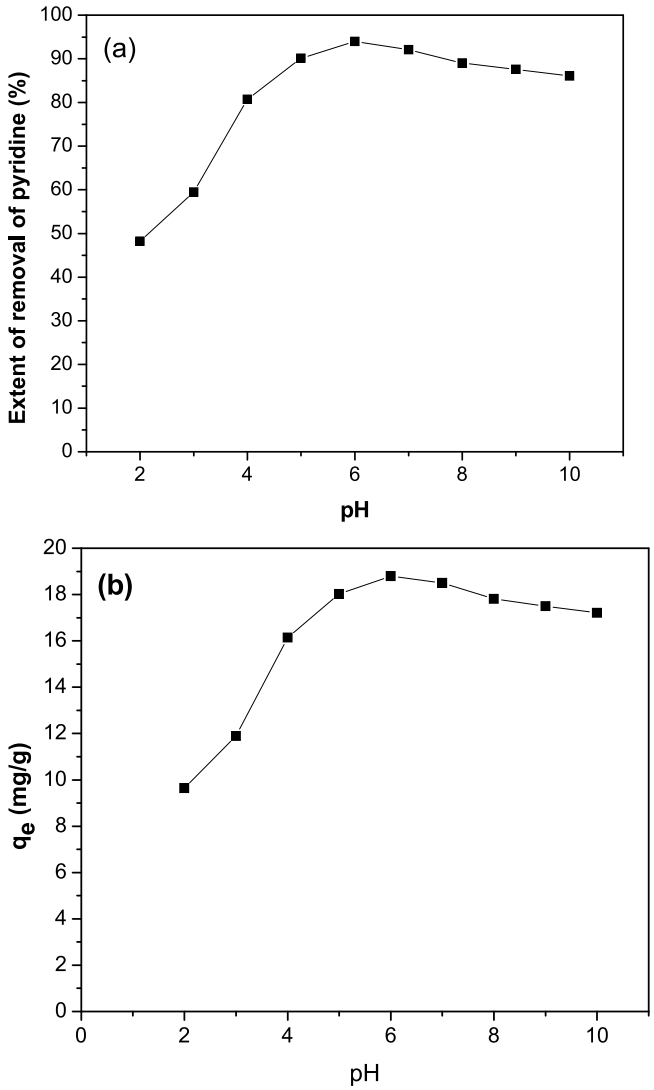

Fig. 6. Effect of pH on the removal of pyridine using TWR adsorbent in ultrasound assisted adsorption (a): extent of removal; (b): amount of pyridine adsorbed at equilibrium (T = 303 K, t = 90 min, c_i = 50 mg/L, w = 2.5 g/L, P = 120 W).

solution at 303 K, pH of 6, time of 90 min and ultrasonic power of 120 W. The results for the influence of TWR loading in the case of ultrasound assisted adsorption are depicted in Figs. 7(a) and 7(b) in terms of the extent of removal and amount of pyridine adsorbed at equilibrium respectively. The obtained findings revealed that the extent of removal of pyridine considerably increased from 39% to 94% with an increase in loading of TWR from 0.5 to 2.5 g/L (Fig. 7(a)) as more number of adsorption sites are available at higher TWR loading. As also shown in Fig. 7(a), for subsequent increase in TWR loading from 2.5 g/L to 4 g/L, no significant change in extent of removal (observed change from 94% to 95.18%) was seen. The trend for adsorption capacities revealed that the adsorption capacity changed from 11.85 mg/g to 18.8 mg/g as depicted in Fig. 7(b) with increasing TWR loading from 0.5 g/L to 2.5 g/L, beyond which marginal change was seen. The observed marginal change in extent of removal at much higher loading is attributed to the overlapping adsorbent sites because of possible agglomeration (Tang et al., 2017). The low adsorbent to adsorbate ratio at low TWR loading leads to more effective utilization of most of the active adsorption sites on TWR giving higher adsorption capacities for a change in TWR loading. At much higher TWR loading, some of active sites remain unutilized as the pyridine molecules are the limiting in the solution. Based on the obtained results, the optimum TWR loading was established as 2.5 g/L where most effective extent of removal as 94% with TWR adsorption capacity of 18.8 mg/g is obtained. The observed trends in present work match with literature depictions. Hashemian and Mirshamsi (2012) reported that the adsorption of 2-picoline increased from 480 mg/g to 505 mg/g with an increase in saw dust adsorbent loading from 0.05 g/L to 0.1 g/L, but further increase in loading of adsorbent from 0.1 g/L to 1 g/L yielded marginal change in the amount of 2-picoline adsorbed. Sarkar and

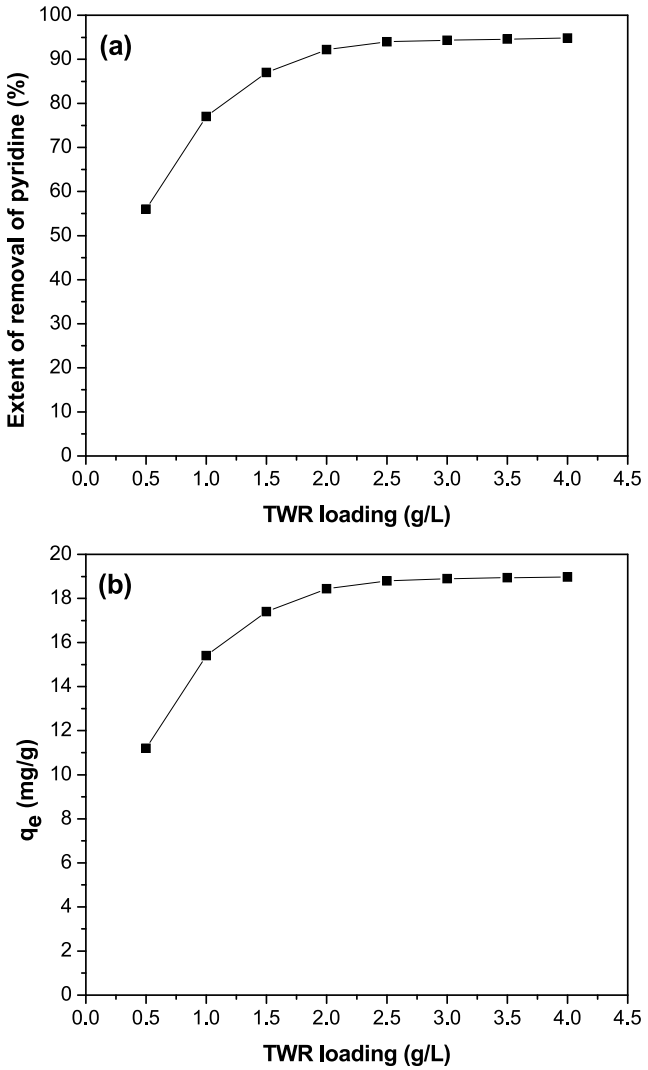

Fig. 7. Effect of TWR loading on the removal of pyridine using ultrasound assisted adsorption (a): extent of removal; (b): amount of pyridine adsorbed at equilibrium (T = 303 K, t = 90 min, pH = 6, P = 120 W, c_i = 50 mg/L).

Sarkar (2019) also demonstrated that the removal of hexavalent chromium on nanocomposite increased from 15% to 85% with a positive change in the nanocomposite quantity from 0.5 g to 3 g in the case of ultrasound assisted adsorption and further increase from 3 g to 5 g did not yield any substantial change in the removal.

3.2.4. Influence of contact time

The trends for the influence of contact time on extent of removal using ultrasound assisted adsorption are depicted in Figs. 8(a) and 8(b). It is observed that removal increases from 70% (q_e = 14 mg/gm) to 94% (q_e = 18.8 mg/gm) for the case of initial concentration of solution as 50 mg/L for a change in contact time from 10 min to 90 min. Similarly for 70 mg/L solution, the observed changes were from 62.1% (q_e = 17.38 mg/gm) to 89% (q_e = 24.92 mg/gm) whereas for 90 mg/L, the change was from 49.1(q_e = 17.90 mg/gm) % to 83.1% (q_e = 29.95 mg/gm) for a similar change in contact time under operating conditions as temperature of 303 K, pH as 6, TWR loading of 2.5 g/L and power dissipation as 120 W. Further increase in contact time from 90 min to 120 min resulted in only marginal change in extent of removal with actual value as 94.3% for 50 mg/L, 89.6% for 70 mg/L and 83.4% for 90 mg/L solutions. Considering that equilibrium is obtained at 90 min, further experiments were performed by keeping 90 min as batch time for ultrasound assisted adsorption.

Experimentation was also performed in conventional batch shaker to understand the effect of contact time. It is observed that pyridine removal increased from 35.1% (q_e = 7.05 mg/gm) to 84.1%(q_e = 16.74 mg/g) for 50 mg/L solution; from 28.2% (q_e = 7.8 mg/g) to 77.9% (q_e = 21.45 mg/g) for 70 mg/L solution and from 23.4% (q_e = 8.4 mg/gm) to 73% (q_e = 26.28 mg/gm) for 90 mg/L pyridine solution with a positive change in contact time from 10 to 160 min as per the

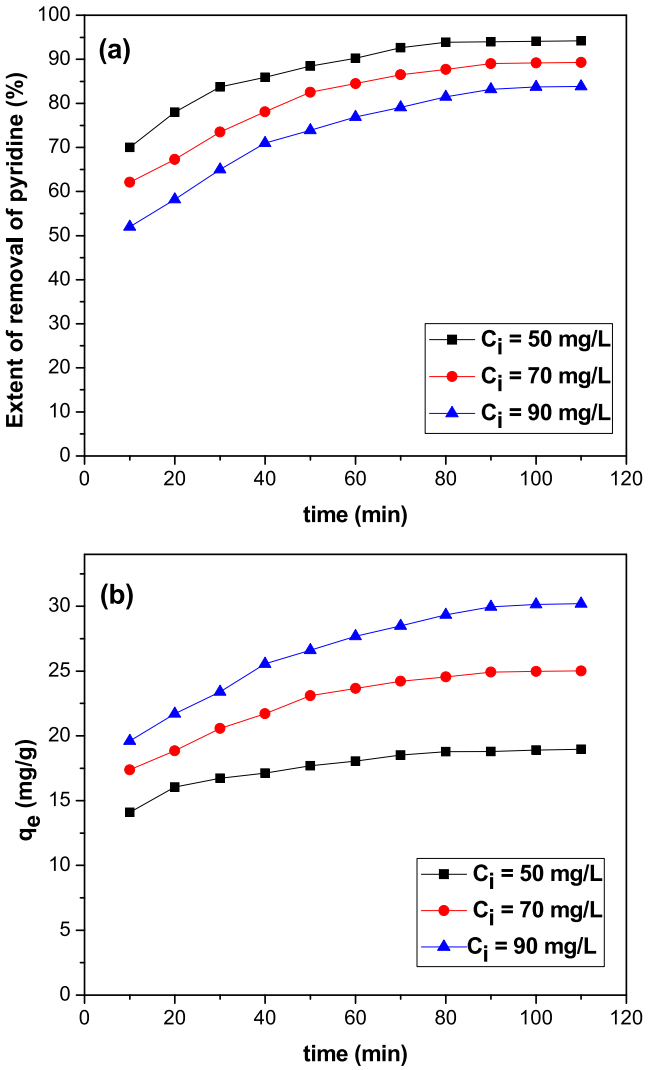

Fig. 8. Effect of contact time on the removal of pyridine using ultrasound assisted adsorption (a): extent of removal; (b): amount of pyridine adsorbed at equilibrium (T = 303 K, pH = 6, w = 2.5 g/L, P = 120 W).

results shown in Fig. 9(a) and 9(b). Increasing contact time subsequently to 200 min resulted in marginal changes in the extent of removal for 50 mg/L, 70 mg/L and 90 mg/L solutions with actual value as 84.3%, 78.05% and 73.6% respectively (Fig. 9(a)). As very little increase in removal was obtained with increasing contact time from 160 min to 200 min, further batch adsorption experiments using the conventional approach were conducted by keeping batch time fixed at 160 min.

It is remarkable to note that during the initial stages, the adsorption of pyridine on TWR is faster as can be easily observed by the steeper curves in the initial stages (Figs. 8(a) and 9(a)) for both ultrasound assisted and conventional approaches of adsorption. Subsequently the rate of adsorption drops as adsorption of pyridine on TWR progresses as can be seen by the flatter curves. It is understood that during early stages abundant vacant sites are available on TWR for faster uptake of pyridine molecule. As the adsorption continues, most of the vacant sites are blocked by pyridine that results in decrease in available vacant sites which resulted in decrease in adsorption rate during lateral stages. Finally very negligible increase in extent of removal of pyridine was observed attributed to established equilibrium. The established equilibrium time for ultrasound assisted adsorption was 90 min whereas for the conventional approach it was 160 min.

The studies for the effects of contact time also allowed establishing that fast and higher removal of pyridine takes place in presence of ultrasound compared to the approach of without ultrasound due to an increased interaction of TWR with pyridine based on the turbulence effects of cavitation. Also the cavitation effects in terms of the acoustic streaming produced during collapse phase of the cavity (Milenkovic et al., 2009) enhance the diffusion leading to higher removal. Similar results are reported by Entezari and Soltani (2008) who investigated ultrasound assisted and conventional adsorption of metals from binary wastewater solution. It was reported that the extent of removal of copper and lead

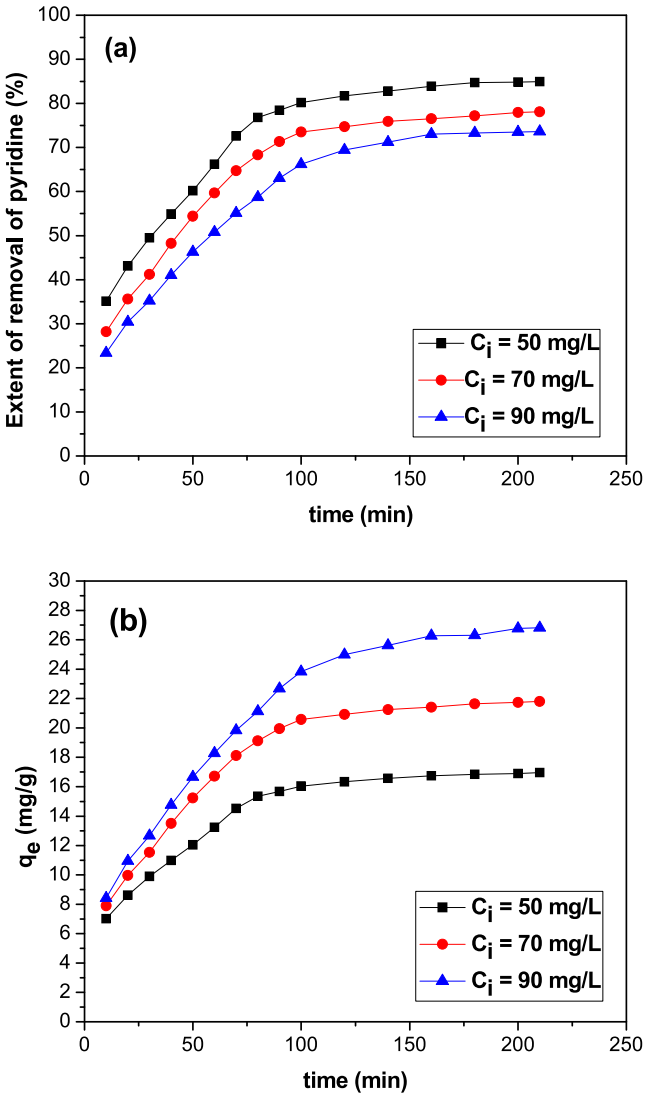

Fig. 9. Effect of contact time on the removal of pyridine using conventional approach of adsorption (a): extent of removal; (b): amount of pyridine adsorbed at equilibrium (pH = 6, w = 2.5 g/L, T = 303 K).

using saffron corm based adsorbent was 34% and 85% respectively for contact time of 6 min using ultrasound assisted adsorption whereas as for conventional batch adsorption method, the extent of removal of copper and lead was 27% and 70% respectively for contact time of 10 min. Gupta and Gogate (2015) also investigated the effect of contact time on extent of removal of copper using watermelon based adsorbent and reported that removal increased from 50% to 90% by increasing contact time from 5 min 20 min but a further increase in contact time to 60 min did not change removal appreciably for the case of ultrasound assisted adsorption. It was also demonstrated that in the absence of ultrasound, copper removal increased from 40 to 86% by increasing time of contact between copper and watermelon from 5 min to 60 min and further increase in contact time to 80 min yielded very less change. It was also reported that the rate of adsorption was high in the initial stages of adsorption similar to that demonstrated in the current work. Again the quantitative differences between the changes in removal extent and equilibrium time as well as intensification due to the use of ultrasound elucidate the importance of the current work.

3.2.5. Influence of initial concentration of pyridine

The dependency of uptake of pyridine on TWR on the changing pyridine initial concentration was studied over the range of 10 mg/L–150 mg/L. The depicted results in Fig. 10 demonstrate that the pyridine removal decreases from 98.2 to 62.3% with a positive change in pyridine concentration over the range of 10 mg/L–150 mg/L under conditions of optimized ultrasonic power, pH, time, dose and applied temperature of 303 K. Similar trends were also observed for conventional

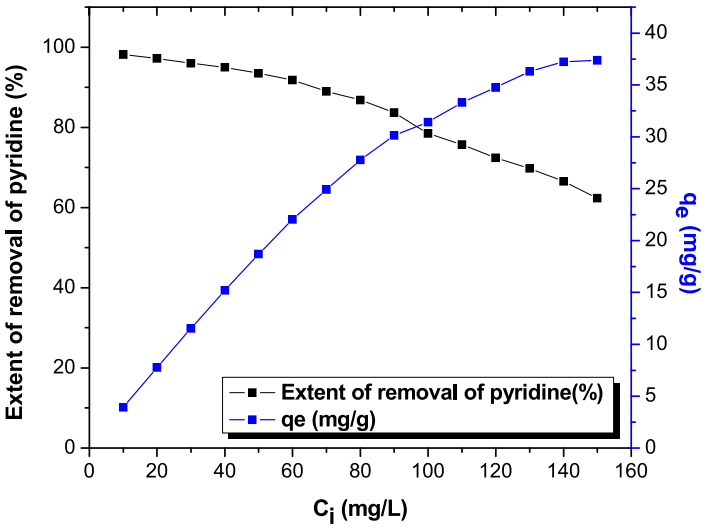

Fig. 10. Effect of initial concentration of pyridine on the extent of removal and amount of pyridine adsorbed at equilibrium using ultrasound assisted adsorption (t = 90 min, T = 303 K, pH = 6, w = 2.5 g/L, P = 120 W).

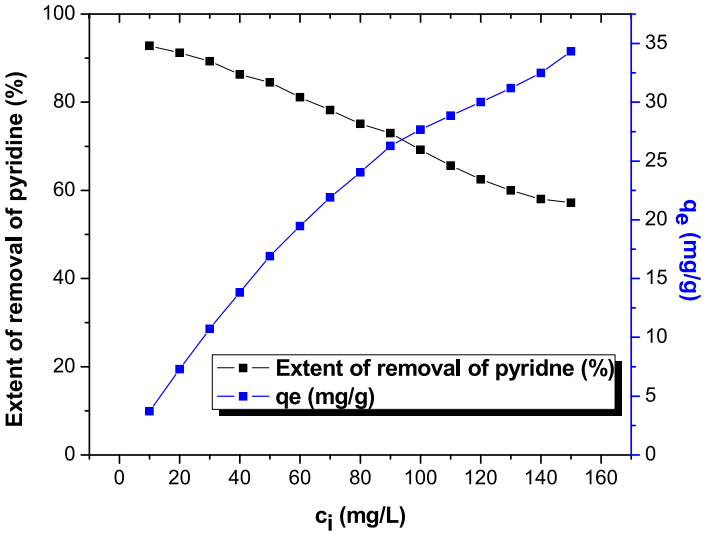

Fig. 11. Effect of initial concentration of pyridine on the extent of removal and amount of pyridine adsorbed at equilibrium using conventional adsorption (t = 160 min, T = 303 K, pH = 6, w = 2.5 g/L).

batch adsorption where the removal decreased from 92.2 to 56.2% (Fig. 11) with a same increase in pyridine concentration from 10 mg/L–150 mg/L. A fixed amount of TWR existing in the solution for all the cases of varying concentrations results in lower removal with increasing concentration of pyridine molecules in the solution.

It is also important to note that the uptake capacity for pollutant showed a different trend. The adsorption capacity for ultrasound assisted adsorption increased from 3.92 mg/g to 37.38 mg/g (Fig. 10) whereas for conventional batch adsorption, the pyridine uptake increased from 3.62 mg/g to 33.72 mg/g (Fig. 11) with a change in initial pyridine content from 10 mg/L to 150 mg/L. The extent of removal of pyridine was higher in the ultrasound assisted approach than conventional batch adsorption method attributed to the acoustic cavitation effects as discussed earlier (Sarkar and Sarkar, 2019). It is also imperative to understand that the uptake adsorption capacity of pyridine increased at higher concentration due to an increase in concentration gradient between TWR surface and bulk of pyridine solution resulting in higher rates of mass transfer for both the approaches of ultrasound assisted and conventional batch adsorption. Djelloula and Hasseine (2013) reported similar trends for methylene blue dye adsorption on milk thistle seed with enhanced dye adsorption capacity at higher concentrations for ultrasound assisted adsorption and conventional batch adsorption. The quantity of dye removed from solution enhanced from 37.68 to 42.82 mg/g for the batch adsorption method without

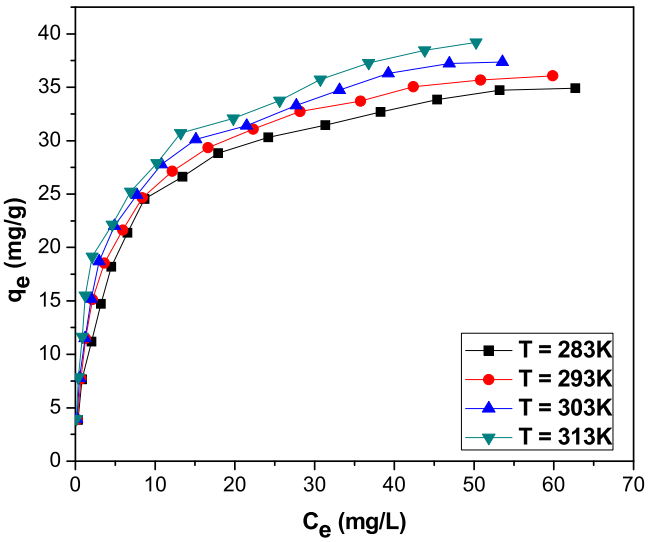

Fig. 12. Equilibrium adsorption capacity of TWR at different equilibrium concentrations and different temperature for the ultrasound assisted adsorption (t = 90 min, pH = 6, w = 2.5 g/L, P = 120 W).

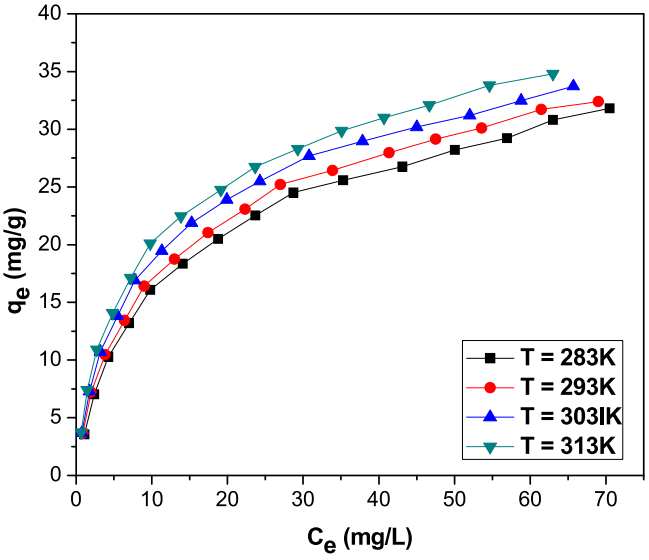

Fig. 13. Equilibrium adsorption capacity of TWR at different equilibrium concentrations and different temperatures for the conventional approach (t = 160 min, pH = 6, w = 2.5 g/L).

ultrasound whereas for ultrasound based adsorption, dye adsorption increased from 68.64 to 150 mg/ g over a change in dye concentration from 50–200 mg/L in both the cases.

3.2.6. Influence of temperature

Figs. 12 and 13 depicts the effect of temperature on adsorption capacity of TWR at different equilibrium concentrations for both ultrasound assisted adsorption and conventional batch adsorption respectively. The pyridine equilibrium uptake for ultrasound assisted adsorption increased from 34.92 mg/g to 39.9 mg/g (Fig. 12) and for conventional batch adsorption, equilibrium adsorption capacity increased from 31.8 mg/g to 34.9 mg/g (Fig. 13) for an increase in temperature from 283 K to 313 K. At higher temperatures, the movement of pyridine increases which resulted in enhancing the adsorption on TWR. The extent of removal observed was again higher for ultrasound assisted adsorption compared to conventional batch adsorption. The effect was seen to be dependent on the temperature as well. The cavitation bubbles are easily formed at higher temperature as viscosity and tensile stress of liquid decreases leading to better results for the adsorption of pyridine

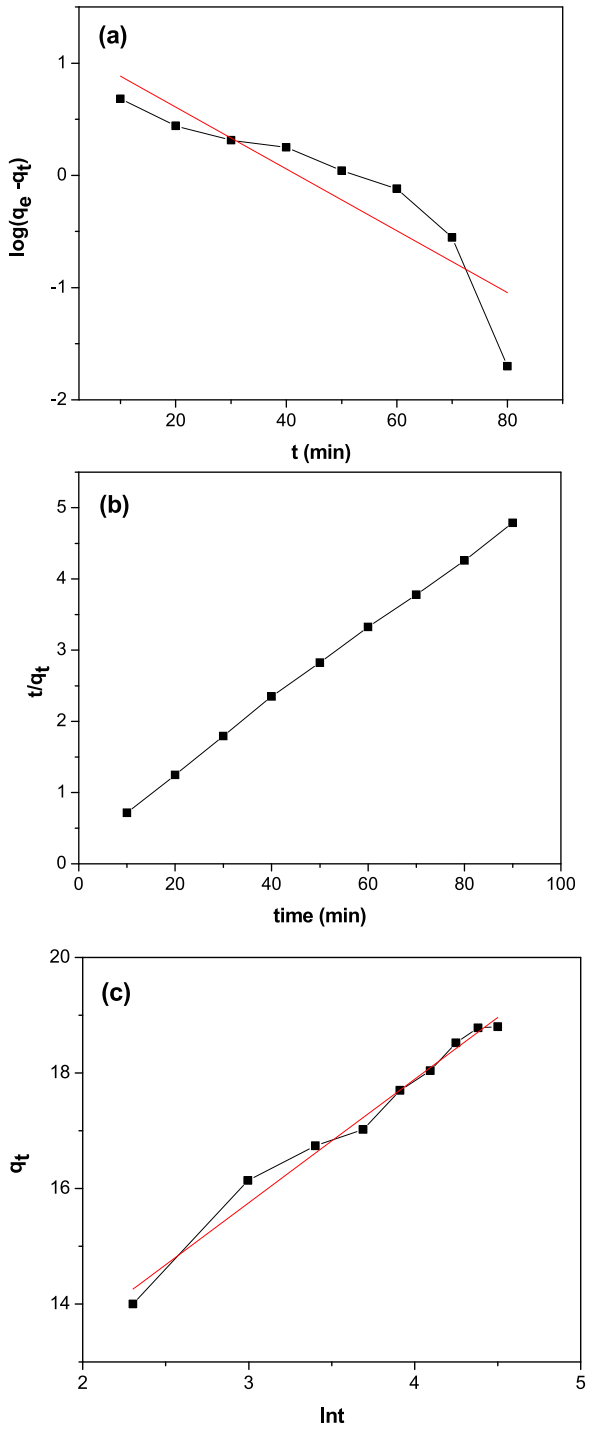

Fig. 14. Kinetic model fitting for batch data obtained for removal of pyridine using ultrasound assisted adsorption under conditions of c_i = 50 mg/L, T = 283 K, pH = 6, w = 2.5 g/L and P = 120 W (a): Pseudo-First order model, (b): Pseudo-Second order model, (c): Elovich model.

on TWR (Gogate et al., 2011). The observed intensification in the adsorption capacity due to the use of ultrasound was about 10% at temperature of 283 K which increased to about 15% at temperature of 313 K.

The higher adsorption capacity at higher temperature for both the methods also concluded the endothermic nature of pyridine adsorption using TWR adsorbent. Sarkar and Sarkar (2019) also reported same trends with capacity of chromium

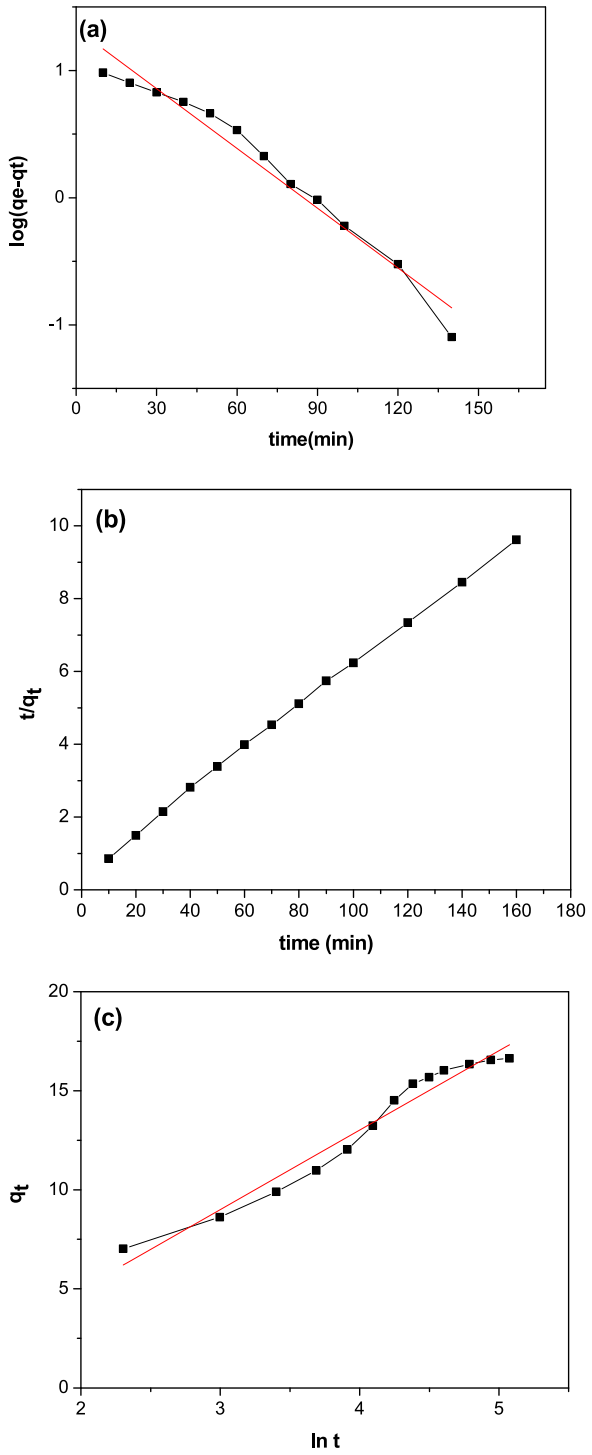

Fig. 15. Kinetic model fitting for batch data obtained for removal of pyridine using conventional adsorption under conditions of $c_i = 50$ mg/L, T = 283 K, pH = 6 and w = 2.5 g/L, (a): Pseudo-First order model, (b): Pseudo-Second order model, (c): Elovich model.

on nanocomposite increasing from 126.5 mg/g to 152 mg/g for conventional batch adsorption and from 200 mg/g to 228 mg/g for ultrasound assisted adsorption for an increasing the temperature from 290 K to 310 K again confirming

Table 1
Kinetic parameters for ultrasound assisted adsorption and conventional adsorption of pyridine using TWR (T = 303k, time for ultrasound assisted adsorption = 90 min, time for conventional adsorption = 160 min, pH = 6, w = 2.5 g/L).

Kinetics	Ci (mg/L)	50		70		90	
		U-ads.	C-ads.	U-ads.	C-ads.	U-ads.	C-ads.
Pseudo-first order	q_{exp} (mg/g)	18.80	16.74	24.92	21.42	29.95	26.28
	q_e (mg/g)	7.561	21.22	15.25	27.6	20.85	30.78
	k_f (min^{-1})	0.042	0.036	0.048	0.0336	0.034	0.025
	R^2	0.944	0.965	0.949	0.970	0.961	0.965
	RMSE	0.400	0.11	0.12	0.105	0.14	0.12
Pseudo-second order	q_{exp} (mg/g)	18.80	16.74	24.92	21.42	29.95	26.28
	q_e (mg/g)	19.50	17.30	25.90	22.00	31.5	28.16
	k_s (min^{-1})	0.011	0.0083	0.0080	0.0060	0.0030	0.0037
	R^2	0.9988	0.9990	0.9988	0.9960	0.9930	0.9970
	RMSE	0.040	0.079	0.027	0.041	0.060	0.096
Elovich Model	α (mg/g min)	153.16	1.875	35.02	1.83	10.30	1.70
	β (g mg^{-1})	0.46	0.24	0.27	0.177	0.17	0.139
	R^2	0.983	0.964	0.974	0.967	0.966	0.967
	RMSE	0.27	0.60	0.38	0.80	0.60	1.02

(* U-ads: Ultrasound assisted adsorption, C-ads: Conventional batch adsorption).

endothermic nature of adsorption. Though the trends can be confirmed easily from literature, there exist quantitative differences in the adsorption capacity for specific adsorbate system establishing the importance of the current work.

3.2.7. Adsorption kinetics

Kinetic model study is important in determining the design parameters useful for exploring the commercial applications. Adsorption kinetic study for ultrasound assisted adsorption and conventional batch adsorption was performed on the basis of obtained experimental data using pseudo 1st order, pseudo 2nd order model and Elovich model. The pseudo 1st order kinetic model equation is depicted as follows (Weber and Morris, 1963; Aruna et al., 2020)

$$\log(q_e - q_t) = \frac{-k_f t}{2.303} + \log q_e \tag{5}$$

Pseudo 2nd order kinetic model equation is depicted as follows (Blanchard et al., 1984).

$$\frac{t}{q_t} = \frac{t}{q_e} + \frac{1}{q_e^2 k_s} \tag{6}$$

Elovich kinetic model equation is depicted as follows (Ghaedi et al., 2015).

$$q_t = \frac{1}{\beta}\ln(\alpha\beta) + \frac{1}{\beta}\ln(t) \tag{7}$$

where, q_e is the maximum amount of pyridine adsorbed on TWR at equilibrium (mg/g) and q_t (mg/g) is the amount of pyridine uptake on TWR at time 't' expressed in min. k_f (min^{-1}) is the rate constant for pseudo 1st order model in and and k_s(mg/g) is the rate constant for pseudo 2nd order kinetic model. α and β are constants for Elovich model where α depicts the chemisorption contribution and β gives the extent of adsorbent surface coverage.

Error analysis was also performed using the approach based on root mean square error (RMSE) function based on the obtained values from the kinetic model to evaluate the best fitting using the following equation (Jain et al., 2020).

$$RMSE = \sqrt{\frac{\sum(y_{observed} - y_{predicated})^2}{n}} \tag{8}$$

Where $y_{observed}$ and $y_{predicted}$ are the experimental and calculated values. n is total experimental points considered for the analysis.

The experimental and predicted values of q_e,rate constants for pseudo 1st order, pseudo 2nd order and the Elovich models along with the obtained values of R^2 and RMSE have been given in Figs. 14 and 15. Table 1 for the ultrasound assisted and conventional batch adsorption approaches. The inconsistency was seen between observed values and calculated values of q_e for Pseudo 1st order model. Also the R^2 values for pseudo 1st order kinetic models were not close to unity (for all concentrations, it was around 0.95). The obtained q_e values and the calculated q_e values were very much nearer for pseudo 2nd order model and also the values of R^2 were close to unity (around 0.99) for both ultrasound assisted and conventional batch adsorption approaches. The obtained R^2 values for Elovich model were around 0.965 for both ultrasound assisted and conventional batch adsorption indicating not so good fitting compared to the pseudo second order model. The RMSE values as shown in Table 1 for pseudo 2nd order model were also very less compared to Elovich and pseudo 1st order models. All these finding confirmed the best fitting of pseudo 2nd order model for both ultrasound

assisted and conventional batch adsorptions. The trends described in present study are matching with the trends reported by Milenkovic et al. (2009) where pseudo 2nd order kinetic model was demonstrated to be best compared to pseudo 1st order kinetic and Elovich model for adsorption of copper in the absence and presence of ultrasound using hazelnut shell based activated carbon.

3.2.8. Evaluation of adsorption isotherms

The application of different isotherm models is essential to understand the adsorption behaviour of TWR for removal of pyridine. Adsorption isotherm was examined using different models as per the discussion offered in this section.

Langmuir model is based on assumption of equal affinity of all sites on the adsorbent for the adsorbate and establishes the governing mechanism of monolayer adsorption process. Langmuir model is explained by following linear equation (Langmuir, 1947; Dil et al., 2016; Gupta et al., 2013).

$$\frac{c_e}{q_e} = \frac{1}{k_L q_m} + \frac{c_e}{\mathrm{q_m}} \tag{9}$$

Where, q_e (mg/g) is equilibrium adsorption capacity of TWR, c_e is equilibrium adsorbate concentration, k_L (L/mg) is the Langmuir constant and $\mathrm{q_m}$ (mg/g) is the maximum adsorption capacity.

Freundlich adsorption isotherm model is based on formation of multilayer adsorption as it describes the heterogeneous system. This model is represented by following linear equation (Freundlich, 1906; Mohammadi et al., 2011).

$$\ln q_e = \ln k_F + \frac{1}{n} \ln c_e \tag{10}$$

Where, $q_e \left(\frac{\mathrm{mg}}{\mathrm{g}}\right)$ represents adsorption capacity of TWR at equilibrium, c_e is equilibrium concentration, k_F is Freundlich constant and $\frac{1}{n}$ is the model parameter. Typically, condition of $\frac{1}{n} > 1$ gives adverse adsorption conditions.

Temkin model is based on assumed interactions between adsorbate–adsorbent such that the heat of adsorption linearly decreases with coverage of adsorbate. Temkin model equation is expressed as follows (Temkin and Pyzhev, 1940).

$$q_e = B \ln k_T + B \ln c_e \tag{11}$$

Where, $B_1 = \frac{\mathrm{RT}}{b}$ is heat of adsorption, k_T is the Temkin model constant signifying adsorbate and adsorbent interaction and q_e is maximum adsorption capacity.

Dubinin–Radushkevich [D–R] isotherm model is represented by following equation (Dubinin and Radushkevich, 1947; Mittal et al., 2010)

$$lnq_e = -B\varepsilon^2 + lnq_{max} \tag{12}$$

Where, q_{max} is maximum adsorption capacity (mg/g), ε is Polanyi potential (kJ/mol), B is D–R isotherm constant and E (kJ/mol) is mean adsorption energy. The value of E can be obtained using following equation:

$$E = \frac{1}{\sqrt{2B}} \tag{13}$$

The D–R model also predicts the behaviour of adsorption based on the values of mean adsorption energy (E). Values of E lesser than 8 (kJ/mol) predict physical adsorption whereas E values greater than 8 (kJ/mol) corresponds to chemical adsorption (Gupta et al., 2014).

The fitting of best isotherm model to the obtained data using experimental studies was examined for both ultrasound assisted and conventional batch absorption using the Average relative error (ARE). The ARE calculation can be represented by following equation (Kapoor and Yang, 1989).

$$\mathrm{ARE} = \frac{100}{n} \sum_{i=1}^{n} \left| \frac{(q_{e,\mathrm{exp}} - q_{e,\mathrm{calc}})}{q_{e,\mathrm{exp}}} \right|_i \tag{14}$$

The obtained data for the ultrasound assisted adsorption is given in Table 2. It can be seen that the obtained q_e values for Langmuir and Temkin isotherm are very close to the experimental values compared to Freundlich isotherm and D–R isotherm. Also the obtained R^2 values for Langmuir (R^2>0.99) and Temkin isotherms (R^2>0.99) are very close to unity compared to Freundlich isotherm (R^2<0.95) and Dubinin–Radushkevich isothermal (R^2<0.78). The ARE values as shown in Table 2 for Langmuir and Temkin are less compared to Freundlich isotherm and Dubinin–Radushkevich isotherms for all the temperatures studied in the work. The comparison of the experimental values of equilibrium adsorption with calculated values for all the isotherms in the case of ultrasound assisted adsorption is depicted in Fig. 16(a). The observations in Fig. 16(a) clearly indicate that the calculated values of Langmuir and Temkin are very close to the experimental values confirming the best fitting obtained by Langmuir and Temkin for ultrasound assisted adsorption of Pyridine on TWR.

Conventional batch adsorption isotherm data was also depicted in Table 2. It was observed that the experimental q_e values and calculated q_e values for Langmuir isotherm are very close to each other compared to Freundlich isotherm, Temkin and D–R isotherms. The obtained R^2 values for Langmuir (R^2>0.99) are very close to unity compared to the

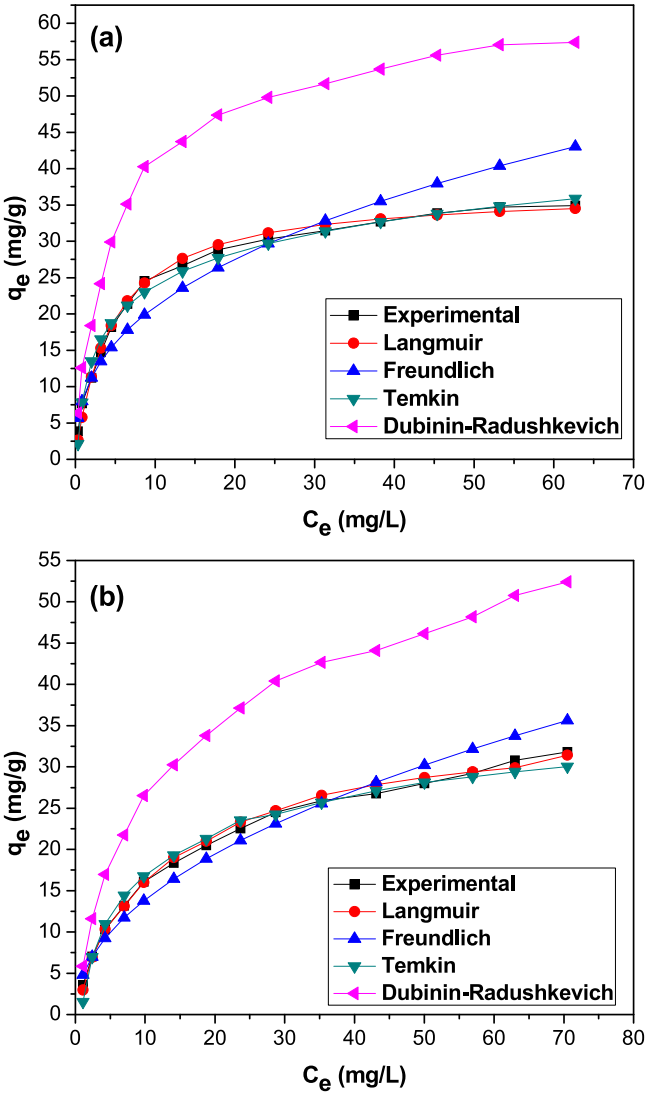

Fig. 16. Comparison of calculated adsorption capacities from different isotherms with experimental values for the removal of pyridine using TWR (a): ultrasound assisted adsorption. (b): conventional adsorption.

Temkin isotherms(R^2< 0.99), Freundlich isotherm (R^2<0.95) and Dubinin–Radushkevich isothermal (R^2<0.78). The ARE values shown in Table 2 for Langmuir isotherm are also less compared to Freundlich, Temkin and Dubinin–Radushkevich isotherms. The comparison of the experimental values of equilibrium adsorption capacity with calculated values for all the isotherms in the case of conventional approach without using ultrasound is given in Fig. 16(b). The observations in Fig. 16(b) clearly indicate that the calculated values of Langmuir are very close to the experimental values confirming the best fitting obtained by Langmuir adsorption. Sarkar and Sarkar (2019) also reported similar results with adsorption of chromium in the presence of ultrasound following Langmuir and Temkin isotherms whereas adsorption in absence of ultrasound following only Langmuir isotherm. Milenkovic et al. (2009) reported that the best fitting was only demonstrated for Langmuir adsorption isotherm for adsorption of copper ions on hazelnut shell based activated carbon both in presence and absence of ultrasound. The varying fitting of the isotherm models depending on the specific system confirm the importance of the presented results in the current work.

3.2.9. Thermodynamic analysis

Thermodynamic parameters, ΔG, ΔH and ΔS were estimated by using the Van't Hoff equation (Gupta et al., 1997) as given below.

$$\ln k = \frac{-\Delta G^0}{RT} = \frac{\Delta S^0}{R} - \frac{\Delta H^0}{R}\frac{1}{T} \tag{15}$$

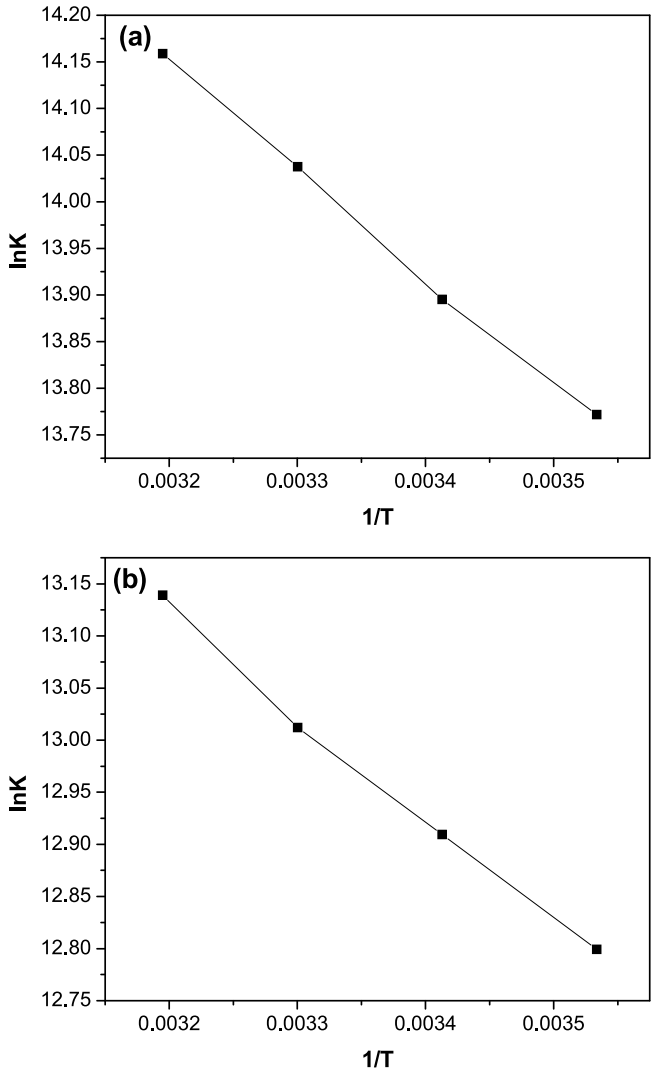

Fig. 17. Vant Hoff's plots for adsorption of pyridine on TWR based on Langmuir model (a): ultrasound assisted adsorption (T = 283 K, pH = 6, w = 2.5 g/L, P = 120 W, t = 90 min) (b): conventional adsorption (T = 283 K, pH = 6, w = 2.5 g/L, t = 160 min).

The isotherm constants k_L, k_F and k_T (L/mg) were converted into required units (L/mol) and multiplied by factor 55.5 (molar concentration of water) (Jain and Gogate, 2018) to make the k values unit less. The obtained values of the thermodynamic parameters for both ultrasound assisted adsorption and conventional shaker based batch adsorption as per the plots represented in Fig. 17 are given in Table 3. The obtained negative ΔG values confirmed the feasibility of both adsorption approaches. With increasing temperature, the obtained ΔG values became more negative representing more spontaneous adsorption mechanism at higher temperature. ΔH values were observed positive for both adsorption approaches confirming the endothermic nature. The obtained ΔH values for both adsorption mechanisms were less than 40 kJ/mol confirming the dominant physical adsorption (Celekli et al., 2012). Similarly, positive ΔS values indicate randomness and increased affinity of pyridine towards TWR. The obtained ΔG, ΔH and ΔS values for ultrasound assisted adsorption were found to be higher compared to conventional batch adsorption as shown in Table 3. These trends clearly demonstrated that ultrasound assisted adsorption is more favourable in terms of feasibility, spontaneous nature and randomness compared to conventional batch adsorption as also reported in the literature (Sarkar and Sarkar, 2019). Entezari and Soltani (2008) also reported similar kind of results for adsorption of copper and lead with endothermic nature and higher feasibility and spontaneity for ultrasound assisted adsorption compared to adsorption in absence of ultrasound based on the obtained values of thermodynamic parameters.

Table 2
Isotherm parameters for ultrasound assisted adsorption and conventional adsorption of pyridine on TWR (time for ultrasound assisted adsorption = 90 min, time for conventional adsorption = 160 min, pH = 6, w = 2.5 g/L).

Isotherm	T (K)	283k		293k		303k		313k	
		U-ads.	C-ads.	U-ads.	C-ads.	U-ads.	C-ads.	U-ads.	C-ads.
Langmuir	k_L (L/mg)	0.220	0.0833	0.267	0.0933	0.287	0.10	0.324	0.117
	q_m (mg/g)	37.00	35.6	38.03	36.24	39.0	36.9	40.48	38.61
	R^2	0.9985	0.9906	0.9981	0.9931	0.9967	0.993	0.997	0.993
	ARE	0.82	0.775	1.22	0.955	2.02	0.947	1.78	1.090
Freundlich	k_F (L/mg)	8.56	4.60	9.40	5.11	10.27	5.63	11.5	6.14
	1/n	0.389	0.481	0.375	0.467	0.367	0.458	0.35	0.449
	R^2	0.942	0.9619	0.938	0.9667	0.952	0.958	0.943	0.967
	ARE	1.97	1.48	2.02	1.39	4.01	1.59	2.32	1.40
Temkin	B_T (mg/g)	6.51	6.96	6.4	6.88	6.3	7.21	6.17	7.19
	k_T (L/mg	3.95	1.13	5.29	1.37	6.99	1.6	8.47	1.79
	R^2	0.990	0.980	0.992	0.981	0.990	0.978	0.991	0.979
	ARE	1.02	1.10	0.91	1.19	1.50	1.60	1.03	1.20
Dubinin– Radushkevich	q_m (mg/g)	57.37	52.42	74.27	53.37	76.81	55.57	83.15	57.07
	E (kJ/mol)	1.53	0.74	1.88	0.90	2.40	1.01	2.67	1.16
	R^2	0.751	0.743	0.753	0.766	0.712	0.733	0.781	0.734
	ARE	9.64	9.72	15.89	9.70	21.98	9.72	16.23	9.60

(* U-ads: Ultrasound assisted adsorption, C-ads: Conventional batch adsorption.)

Table 3
Thermodynamic parameters for ultrasound assisted adsorption and conventional adsorption of pyridine on TWR at different temperatures.

Isotherm	ΔG^0 (kJ/mol)								ΔH^0 kJ/mol		ΔS^0 kJ/mol k	
	283k		293k		303k		313k					
	U-ads.	C-ads.	U-ads.	C-ads.	U-ads.	C-ads.	U-ads.	C-ads.	U-ads.	C-ads.	U-ads.	C-ads.
Langmuir	−32.44	−30.11	−34.00	−31.42	−35.26	−32.69	−36.83	−34.16	9.115	8.015	0.14	0.134
Freundlich	−41.00	−39.55	−42.6	−41.91	−44.37	−42.82	−46.11	−44.49	7.15	7.00	0.17	0.165
Temkin	−39.91	−36.23	−41.31	−37.97	−43.43	−39.67	−44.88	−41.29	12.11	11.51	0.18	0.169

(* U-ads: Ultrasound assisted adsorption, C-ads: Conventional batch adsorption.)

3.2.10. Comparison of Maximum extent of pyridine removal using different adsorbents

Table 4 depicts the comparison of the obtained percentage removal using ultrasound assisted adsorption and conventional batch adsorption in the present work with the literature. The maximum extent of removal obtained in present work is 98.2% by ultrasound assisted adsorption and 92.2% by conventional batch adsorption method. Comparison with the studies reported in literature established that the extent of removal was high compared with the other adsorbents reported in the literature. The comparison allows establishing good efficacy for the TWR adsorbent and the ultrasound assisted approach reported in the present work.

4. Conclusions

Present study deals with the exploring the potential of tea waste residue (TWR) for treatment of pyridine containing wastewater using ultrasound assisted adsorption and conventional batch adsorption. The optimum operating conditions were established for both the approaches of ultrasound assisted and conventional batch adsorption. The maximum amount of pyridine adsorbed using ultrasound and conventional batch adsorption were 39.9 mg/g and 34.8 mg/g with the maximum extent of pyridine removal as 98.2% and 92.2% respectively. The kinetic study indicated that pseudo-second order model best fitted for both type of adsorption representing the rate-limiting step as chemical interaction between functional groups on TWR and pyridine molecules. The isotherm data analysis showed that the Langmuir model and Temkin model were best fitted for adsorption of pyridine using ultrasound assisted approach whereas Langmuir model was found to be more suitable for conventional batch adsorption. The thermodynamic study confirmed that both the adsorption approaches are endothermic, feasible and spontaneous. Thus the present work clearly established the utility of TWR as an effective adsorbent and also demonstrated the intensification benefits for the ultrasound assisted adsorption compared to conventional batch adsorption based on fast equilibrium attainment, higher extent of removal, feasibility and spontaneity.

Table 4
Comparison of maximum extent of pyridine removal using different adsorbents.

Adsorbents	Maximum extent of removal of pyridine from wastewater	Reference
Tea waste residue (TWR)	98.2% (Ultrasound assisted adsorption)	Present work
Tea waste residue (TWR)	92.25% (Conventional batch adsorption)	Present work
Bagasse Fly Ash(BFA)	98.2%	Lataye et al. (2006)
Activated carbon from coconut shell.	96.5%	Mohan et al. (2004)
Rich Husk Ash	97%	Lataye et al. (2008a,b)
Granular activated carbon	96%	Lataye et al. (2008a,b)
Rundle oil shale	10%	Zhu et al. (1988)
Na-montmorillonite	25%	Baker and Luh (1971)
Porous hydroapatite	88%	Bouyarmane et al. (2010)
Activated carbon cloth	75%	Zhu et al. (2016)
Combusted oil shale	15%	Essington (1992)
Chitosan biocomposite	96. 5%	Bageru and Srivastava (2019)
Alginate biocomposite	90%	Bageru and Srivastava (2019)
Natural apatite	40.2%	Bouyarmane et al. (2010)
Synthetic apatite	46.2%	Bouyarmane et al. (2010)
MN 200	49.1	Zhu et al. (2016)
MN 500	79.1%	Zhu et al. (2016)
Lignosuflonate	87.9%	Xia et al. (2018)
Sodium kaoline	12%	Baker and Luh (1971)
Sodium montmorillonite	67%	Baker and Luh (1971)

CRediT authorship contribution statement

Gaurav B. Daware: Methodology, Investigation, Writing - original draft. **Parag R. Gogate:** Conceptualization, Supervision, Writing - review & editing, Project administration.

Declaration of competing interest

The authors declare that they have no known competing financial interests or personal relationships that could have appeared to influence the work reported in this paper.

Acknowledgement

Authors are thankful to University Grants Commission (UGC), New Delhi, India for support under UGC-NRC at the Institute of Chemical Technology, Mumbai, Maharashtra, India.

References

Ahmaruzzaman, M., Gupta, V.K., 2011. Rice husk and its ash as low-cost adsorbents in water and wastewater treatment. Ind. Eng. Chem. Res. 50 (24), 13589–13613.
Akita, S.S., Takeuchi, H., 1993. Sorption equilibria of pyridine derivatives in aqueous solution on porous resins and ion exchange resins. J. Chem. Eng. Jpn. 26, 237–241.
Alam, T., Kamaluddin, 2000. Interaction of 2-amino, 3-amino and 4-aminopyridines with chromium and Manganese Ferro cyanides. J. Colloid Interface Sci. 224, 133–139.
Aruna, J.V., Shanmugavel, R., Abraham, N., Deepalakshmi, S., Sivakumar, P., 2020. Kinetic studies validated by artificial neural network simulation for the removal of dye from simulated wastewater by the activated carbon produced from acalypha indica leaves. Environ. Technol. Innov. 53, 101244.
Bageru, A.B., Srivastava, V.C., 2019. Efficient teff-straw based biocomposite with chitosan and alginate for pyridine removal. Int. J. Environ. Sci. Technol. 16, 5757–5766.
Bai, Y., Sun, Q., Zhao, C., Wen, D., Tang, X., 2009. Aerobic degradation of pyridine by a new bacterial strain, Shinella Zoogloeoides BC026. J. Ind. Microbial Biotechnol. 36, 1391–1400.
Baker, R.A., Luh, M.D., 1971. Pyridine sorption from aqueous solution by montmorillonite and kaolinite. Water Res. 5 (10), 839–848.
Bhandari, P.S., Gogate, P.R., 2018. Kinetic and thermodynamic study of adsorptive removal of sodium dodecyl benzene sulfonate using adsorbent based on thermo-chemical activation of coconut shell. J. Mol. Liq. 252, 495–505.
Blanchard, G., Maunaye, M., Martin, G., 1984. Removal of heavy metals from water by means of natural zeolites. Water Res. 18, 1501–1507.
Boehm, H.P., 2002. Surface oxide on carbon and their analysis: A critical assessment. Carbon 40, 145–149.
Bouyarmane, H., Asri, S.El., Rami, A., Roux, C., Mahly, M.A., Saoiabi, A., 2010. Pyridine and phenol removal using natural and synthetic apatites as low cost sorbents: influence of porosity and surface interactions. J. Hazard. Mater. 181, 736–774.
Burakova, A.E., Galunina, E.V., Burakovaa, I.V., Kucherovaa, A.E., Agarwalb, S., Tkacheva, A.G., Gupta, V.K., 2018. Adsorption of heavy metals on conventional and nanostructured materials for wastewater treatment purposes: A review. Eco. Environ. Safety 148, 702–712.
Celekli, A., Ilgün, G., Bozkurt, H., 2012. Sorption equilibrium, kinetic, thermodynamic, and desorption studies of reactive red 120 on characontraria. Chem. Eng. J. 191, 228–235.

Daware, G.B., Gogate, P.R., 2020a. Sonochemical degradation of 3-methylpyridine (3MP) intensified using combination with various oxidants. Ultrason. Sonochem. 67, 105–120.
Daware, G.B., Gogate, P.R., 2020b. Adsorption of 3-aminopyridine (3Ap) from aqueous solution using sugarcane bagasse activated carbon (SBAC). Environ. Technol. Innov. 19, 100921.
Daware, G.B., Vijay Babu, P.V., Pangarker, B.L., 2014. Adsorption of 2-picoline from wastewater by agro coal ash: parametric, kinetic, equilibrium and thermodynamic features. Desal. Water Treat. 52, 6263–6270.
Dil, E.A., Ghaedi, A.M., Asfaram, A., Goudarzi, A., Hajati, S., Soylak, M., Agarwal, S., Gupta, V.K., 2016. Modeling of quaternary dyes adsorption onto ZnO–NR–AC artificial 3 neural network: Analysis by derivative spectrophotometry. J. Ind. Eng. Chem. 34, 186–197.
Djelloula, C., Hasseine, A., 2013. Ultrasound-assisted removal of methylene blue from aqueous solution by milk thistle seed. Desal. Water Treat. 51, 5805–5812.
Dubinin, M.M., Radushkevich, L.V., 1947. The equation of the characteristic curve of the activated charcoal. Chem. Zentr. 1, 875.
Elsayed, M.A., 2015. Ultrasonic removal of pyridine from wastewater: optimization of the operating conditions. Appl. Water Sci. 5, 221–227.
Entezari, M.H., Soltani, T., 2008. Simultaneous removal of copper and lead ions from a binary solution by sono-sorption process. J. Hazard. Mater. 160, 88–93.
Essington, M.E., 1992. Adsorption of pyridine by combusted oil shale. Environ. Geol. Water Sci. 19, 83–89.
Fidel, R.B., D.A., Laird., Thompson, M.L., 2013. Evaluation of modified Boehm titration methods for use with biochars. J. Environ. Qual. 42, 1771–1778.
Freundlich, H.M.F., 1906. Over the adsorption in solution. J. Phys. Chem. 57, 385–470.
Gero, A., Markham, J.J., 1951. Studies on pyridines: I. The basicity of pyridine bases. J. Org. Chem. 16, 1835–1838.
Ghaedi, M., Hajjati, S., Mahmudi, Z., Tyagi, I., S., Agarwal., Maity, A., Gupta, V.K., 2015. Modeling of competitive ultrasonic assisted removal of the dyes – Methylene blue and Safranin-O using Fe3O4 nanoparticles. Chem. Engg. J. 268, 28–37.
Girisha, C.R., Singha, P., Kumar Goyal, A., 2017. Removal of phenol from wastewater using tea waste and optimization of conditions using response surface methodology. Int. J. App. Eng. Res. 13, 3857–3863.
Gogate, P.R., Sutkar, V.S., Pandit, A.B., 2011. Sonochemical reactors: important design and scale up considerations with a special emphasis on heterogeneous systems. Chem. Eng. J. 166, 1066–1082.
Gupta, V.K., Ali, I., Saleh, T.A., Siddiqui, M.N., Agarwal, S., 2013. Chromium removal from water by activated carbon developed from waste rubber tires. Environ. Sci. Pollut. Res. 20, 1261–1268.
Gupta, H., Gogate, P.R., 2015. Intensified removal of copper from waste water using activated watermelon based biosorbent in the presence of ultrasound. Ultrason. Sonochem. 30, 113–122.
Gupta, V.K., Jain, R., Nayak, A., Agarwal, S., Shrivastava, M., 2011. Removal of the hazardous dye -Tartrazine by photo degradation on titanium dioxide surface. Mater. Sci. Eng. C 31, 1062–1067.
Gupta, V.K., Nayak, A., Agarwal, S., 2015. Bioadsorbents for remediation of heavy metals: Current status and their future prospects. Environ. Eng. Res. 20, 1–18.
Gupta, V.K., Nayak, A., Agarwal, S., Tyagi, I., 2014. Potential of activated carbon from waste rubber tire for the adsorption of phenolics: Effect of pre-treatment conditions. J. Colloid Interface Sci. 417, 420–430.
Gupta, V.K., Rastogi, A., Dwivedi, M.K., Mohan, D., 1997. Process development for the removal of zinc and cadmium from wastewater using slag-A blast furnace waste material. Sep. Sci. Techn. 32, 2883–2912.
Hashemian, S., Mirshamsi, M., 2012. Kinetic and thermodynamic of adsorption of 2-picoline by sawdust from aqueous solution. J. Ind. Eng. Chem. 18, 2010–2015.
Jain, S.N., Gogate, P.R., 2018. Efficient removal of acid green dye from waste water using activated PrunusDulcis as adsorbent: Batch and column study. J. Environ. Manag. 210, 226–238.
Jain, S.N., Tamboli, S.R., Sutar, D.S., Jadhav, S.R., Marathe, J.V., Shaikh, A.A., Prajapati, A.A., 2020. Batch and continuous studies for adsorption of anionic dye onto waste tea residue: Kinetics, equilibrium, breakthrough and reusability studies. J. Cleaner Prod. 252, 119778.
Jampa, S.S., Unnarkat, A.P., Vanshpati, R., Sivakumar, P., Sinha, M.K., Dharaskar, S., 2020. Adsorption and recyclability aspects of humic acid using nano-ZIF-8 adsorbent. Environ. Technol. Innov. 19, 100927.
Janani, V.A., Saravanan, S., Rajesh, S., Sivakumar, P., Anirbid, S., 2019. Batch and column studies on the removal of methyl orange by acalypha indica biomass using gravitational search algorithm as an optimization tool. Desal. Water Treat. 147, 385–397.
Kalijadis, A.M., Vukcevic, M.M., Jovanovic, Z.M., Lausevic, Z.V., Lausevic, M.D., 2011. Characterisation of surface oxygen groups on different carbon materials by the boehm method and temperature-programmed desorption. J. Serb. Chem. Soc. 76 (5), 757–768.
Kapoor, A.R., Yang, T., 1989. Correlation of equilibrium adsorption data of condensable vapours on porous adsorbents. Gas Sep. Purif. 3, 187–192.
Kumar, R., Mishra, I.M., Mall, I.D., 1995. Treatment of pyridine bearing wastewater using activated carbon. Res. Ind. 40, 33–38.
Landi, M., Naddeo, V., Belgiorno, V., 2010. Influence of ultrasound on phenol removal by adsorption on granular activated carbon. Desal. Water Treat. 23, 181–186.
Langmuir, I., 1947. The adsorption of gases on plane surfaces of glass, mica and platinum. J. Am. Chem. Zentr. 1, 875.
Lataye, D.H., Mishra, I.M., Mall, I.D., 2006. Removal of pyridine from aqueous solution by adsorption on bagasse fly ash. Ind. Eng. Chem. Res. 45, 3934–3943.
Lataye, D.H., Mishra, I.M., Mall, I.D., 2008a. Pyridine sorption from aqueous solution by rice husk ash (RHA) and granular activated carbon (GAC): Parametric, kinetic, equilibrium and thermodynamic aspects. J. Hazard. Mater. 154, 858–870.
Lataye, D.H., Mishra, I.M., Mall, I.D., 2008b. Adsorption of 2-picoline onto bagasse fly ash from aqueous solution. Chem. Eng. J. 138, 35–46.
Lataye, D.H., Mishra, I.M., Mall, I.D., 2009. Adsorption of α-picoline onto rice husk ash and granular activated carbon from aqueous solution: Equilibrium and thermodynamic study. Chem. Eng. J. 147, 139–149.
Malkoc, E., Nuhoglu, Y., 2006. Fixed bed studies for the sorption of chromium (VI) onto tea factory waste. Chem. Eng. Sci. 61, 4363–4372.
Milenkovic, D.D., Dašic, P.V., Veljkovic, V.B., 2009. Ultrasound-assisted adsorption of copper (II) ions on hazelnut shell activated carbon. Ultrason. Sonochem. 16, 557–563.
Mittal, A., Mittal, J., Malviya, Arti, Gupta, V.K., 2010. Removal and recovery of Chrysoidine Y from aqueous solutions by waste materials. J. Colloid Interface Sci. 344, 497–507.
Mohammadi, N., Khani, H., Gupta, V.K., Amereh, E., Agarwal, S., 2011. Adsorption process of methyl orange dye onto mesoporous carbon material–kinetic and thermodynamic studies. J. Colloidal Interface Sci. 362 (2), 457–462.
Mohan, D., Singh, P., Ghosh, D., 2004. Removal of pyridine from aqueous solution using low cost activated carbons derived from agricultural waste materials. Carbon 42, 2409–2421.
Mohan, D., Singh, P., Ghosh, D., 2005. Removal of α-picoline, β-picoline, and γ-picoline from synthetic wastewater using low cost activated carbons derived from coconut shell fibers. Environ. Sci. Technol. 39, 5076–5086.
Nekouei, F., Tayagi, I., Gupta, V.K., 2015. Kinetic, thermodynamic and isotherm studies for acid blue 129 removal 2 from liquids using copper oxide nanoparticle-modified activated carbon as a novel adsorbent. J. Mol. Liq. 201, 124–133.
Pirbazari, A.E., Saberikhah, E., Badrouh, M., Emami, M.S., 2014. Alkali treated foumanat tea waste as an efficient adsorbent for methylene blue adsorption from aqueous solution. Water Res. Ind. 6, 64–80.

Saleh, T.A., Gupt, V.K., 2012. Photo-catalyzed degradation of hazardous dye methyl orange by use of a composite catalyst consisting of multi-walled carbon nanotubes and titanium dioxide. J. Colloid Interface Sci. 371, 101–106.
Saleh, T.A., Gupt, V.K., 2014. Processing methods characteristics and adsorption behavior of tires derived carbons: A review. Adv. Colloid interface 211, 92–110.
Saravanan, R., Karthikeyan, S., Gupta, V.K., Sekaran, G., Narayanan, V., Stephen, A., 2013a. Enhanced photocatalytic activity of ZnO/CuO nanocomposite for the degradation of textile dye on visible light illumination. Mat. Sci. Eng. C 33, 91–98.
Saravanan, P., Sivekumar, P., Geoprincy, G., Gandhi, N., Renganathan, S., 2012. Biosorption of acid green 1 using dried Rhodoturula glutinis biomass. Indian J. Environ. Prot. 32, 207–214.
Saravanan, R., Thirumal, E., Gupta, V.K., Narayanan, V., Stephen, A., 2013b. The photocatalytic activity of ZnO prepared by simple thermal decomposition method at various temperatures. J. Mol. Liq. 177, 394–401.
Sarkar, S., Sarkar, M., 2019. Ultrasound assisted batch operation for the adsorption of hexavalent chromium onto engineered nanobiocomposite. Heliyon 5 (4), e01491.
Shahnaz, T., Vishnu, P.V., Sivakumar, P., Narayanasamy, S., Nanocellulose, 2020. Extracted from grass for adsorption abatement of Ciprofloxacin and Diclofenac removal with phyto, and fish toxicity studies, 268, 115494.
Stern, M., Elmar, H., Kut, O., Hungerbbuhler, K., 1997. Removal of substituted pyridines by combined ozonation/fluidized bed biofilm treatment. Water Sci. Technol. 35, 329–335.
Tang, C.F., Shu, Y., Zhang, R.Q., Li, X., Song, J.F., Zhang, Li B., Ou, Y.T., 2017. Comparison of the removal and adsorption mechanisms of cadmium and lead from aqueous solution by activated carbons prepared from Typhaangustifolia and Salix matsudana. RSC Adv. 26, 16092–16103.
Temkin, M.I., Pyzhev, V., 1940. Kinetics of ammonia synthesis on promoted iron catalyst. Acta. Physico Chem. URSS 12, 327–356.
Weber, W.J., Morris, J.C., 1963. Kinetics of adsorption on carbon from solution. J. Sanit. Eng. Div. Am. Soc. IV Eng. 89, 31–60.
Xia, M., Jin, C., Kong, X., Jiang, M., Lei, D., Lei, X., 2018. Green removal of pyridine from water via adsolubilization with lignosulfonate intercalated layered double hydroxide. Ads. Sci. Tech. 36, 982–998.
Zalat, O.A., Elsayed, M.A., 2013. A study on microwave removal of pyridine from wastewater. J. Env. Chem. Eng. 1, 137–143.
Zhang, C., Li, M., Luo, L.H., Zhang, R., 2009. Pyridine degradation in the microbial fuel cells. J. Hazard. Mater. 172, 465–471.
Zhu, S., Bell, P.R.F., Greenfield, P.F., 1988. Adsorption of pyridine onto spent rundle oil shale in dilute aqueous solution. Water Res. 22, 1331–1337.
Zhu, Q., Moggride, G.D., Agostino, C.D., 2016. Adsorption of pyridine from aqueous solutions by polymeric adsorbents MN 200 and MN 500. Part 2: Kinetics and diffusion analysis. Chem. Eng. J. 306, 1223–1233.